Ultrahigh-contrast imaging by temporally modulated stimulated emission depletion

L.V. Doronina-Amitonova,[1,2,3] I.V. Fedotov,[1,2,4] and A.M. Zheltikov[1,2,4,5,]*

[1]*Physics Department, International Laser Center, M.V. Lomonosov Moscow State University, Moscow 119992, Russia*

[2]*Russian Quantum Center, ul. Novaya 100, Skolkovo, Moscow Region 143025, Russia*

[3]*Current address: Complex Photonic Systems, MESA+ Institute for Nanotechnology, University of Twente, Enschede, The Netherlands*

[4]*Department of Physics and Astronomy, Texas A&M University, College Station, Texas 77843, USA*

[5]*Kurchatov Institute National Research Center, Moscow 123182, Russia*

*Corresponding author: zheltikov@physics.msu.ru

Stimulated emission depletion (STED) is the key optical technology enabling super-resolution microscopy below the diffraction limit. Here, we demonstrate that modulation of STED in the time domain, combined with properly designed lock-in detection, can radically enhance the contrast of fluorescent images of strongly autofluorescent biotissues. In our experiments, the temporally modulated STED technique, implemented with low-intensity continuous-wave laser sources, is shown to provide an efficient all-optical suppression of a broadband fluorescent background, allowing the contrast of fluorescent images of mammal brain tissues tagged with nitrogen-vacancy diamond to be increased by five orders of magnitude. © 2015 Optical Society of America

OCIS codes: (180.2520) Fluorescence microscopy; (170.0110) Imaging systems.

http://dx.doi.org/10.1364/OL.40.000725

Diamond with nitrogen–vacancy (NV) centers offer much promise for quantum technologies [1–3], enable a unique modality of optical magnetometry on the nanoscale [4,5], and allow optical thermometry to be implemented with a millikelvin accuracy and an unprecedented, nanometer-scale spatial resolution, thus providing a unique tool for thermometry of living cells [6]. Diamond nano- and micro-particles with NV centers find growing applications as nonbleaching, cytocompatible labeling agents and cellular biomarkers in bioimaging with standard, linear [7,8], and two-photon [9] laser excitation. The integration of the NV diamond with optical fibers [10,11] helps manipulate, polarize, and interrogate the spin of NV centers through a fiber [12], paving the way toward fiber-format single-photon emitters, quantum sensors, optical magnetometers [13,14], and thermometers [15].

The unique photophysics of NV centers in diamond proves to be ideally suited for stimulated emission depletion (STED) microscopy [16–18], a technique that enables an unprecedented far-field spatial resolution, well below the diffraction limit, leading to revolutionary breakthroughs in optical imaging. When applied to NV centers in diamond, STED microscopy has been shown to yield point-spread functions of only 5.8 nm in width [19,20], helping to resolve individual nitrogen vacancy centers in diamond nanocrystals [21] and allowing a far-field spatial resolution two orders of magnitude higher than the wavelength of excitation light [19]. Wide-field multispectral super-resolution imaging has also been demonstrated [22] using spin-dependent fluorescence in nanodiamonds modulated through the magnetic resonance of NV centers.

Detecting fluorescent markers against a bright autofluorescence of biotissues is one of the key issues in fluorescence microscopy. As a possible solution to this problem, discrimination of the fluorescent signal from autofluorescence using fluorescence of NV centers modulated by a microwave field [23] or a strong alternating magnetic field [24,25] has been demonstrated. Here, we show that temporally modulated STED (TMSTED), combined with properly designed lock-in detection, can help discriminate fluorescence of NV-diamond markers from an intense autofluorescence background, offering an all-optical method of ultra-high-contrast imaging with no need for an additional microwave or a magnetic field, which may have unwanted effects in *in vivo* work. As our experiments show, the TMSTED technique can enhance the contrast of fluorescent images of NV-diamond nanoparticles in autofluorescent mammal brain tissues by five orders of magnitude, providing a powerful tool for ultrahigh-contrast bioimaging.

In our experiments, micro- and nano-particles of diamond with NV centers were used as fluorescent markers. The fluorescence of NV diamond was induced by 532 nm, 5 mW continuous-wave second-harmonic output of a Nd:YAG laser (Fig. 1). This field transfers NV centers from their ground, ^3A state to an excited, ^3E state [green arrow in Fig. 2(a)], which tends to decay with a lifetime of about 11.6 ns, emitting fluorescence [red arrow in Fig. 2(a)] within the range of wavelengths from approximately 600 to 850 nm. Similar to the earlier STED work on
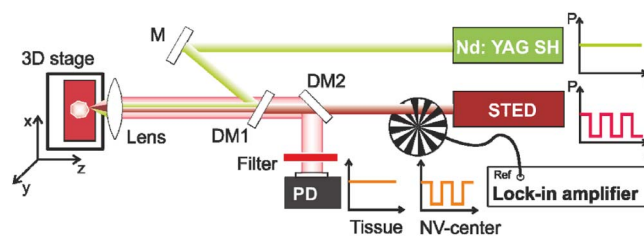

Fig. 1. Experimental setup for TMSTED imaging: Nd:YAG SH, second-harmonic output of a continuous-wave Nd:YAG laser; STED, wavelength tunable source of STED radiation; DM1, DM2, dichroic mirrors; M, mirror; PD, photodetector; Ref, the reference input of the lock-in amplifier.

NV diamond [19–21], this fluorescence emission was suppressed in our experiments through a STED process [red arrow in Fig. 2(a)] using an additional optical field in the near-infrared. In our scheme, this STED field was delivered either by a Ti: sapphire laser or a Ti: sapphire-laser-pumped optical parametric oscillator (OPO), supporting a wavelength tunability range from 800 to 1300 nm.

The STED field is modulated in our experimental scheme with a modulation frequency of 415 Hz and a duty cycle of 50% using a chopper (Fig. 1). The fluorescence signal from NV diamond is detected using a lock-in amplifier, which was set to pick up an input signal at 415 Hz, thus measuring the difference $I_{\text{lock-in}} = I_0 - I_s$ (Fig. 1) between the overall fluorescence signal in the absence of the STED field, I_0, and the fluorescence signal suppressed by STED, I_s. The fluorescence from NV centers is separated from the STED radiation using shortpass filters with a cutoff at 750 nm and a dichroic mirror (DM2 in Fig. 1), providing a reflection coefficient higher than 97% in the range of wavelengths from 400 to 690 nm and transmission in excess of 92% in the 710–1200 nm wavelength range. A notch filter is used to block reflected and scattered 532 nm radiation in front of the detection system. For fluorescent imaging, both excitation and STED laser beams are focused with a 20× micro-objective. A sample is placed on a high-precision three-coordinate translation stage (Fig. 1), which enables scanning along the x- and y-coordinates in the transverse

plane and helps to adjust the position of the sample relative to the beam focus along the z-coordinate.

In the first series of experiments, we examined the performance of the TMSTED detection scheme by measuring the lock-in output for NV diamond on a substrate without any fluorescence background as a function of the power and the wavelength of STED radiation. Typical results of such measurements, performed on an diamond particle with a diameter of about 250 μm, are presented in Fig. 2(b). The efficiency of luminescence signal suppression in STED is an exponential function of the STED field intensity I_{STED} [23], $\eta = \exp(\sigma I_{\text{STED}})$, where σ is the cross section of the stimulated process, giving rise to a lock-in amplifier output $S \propto 1 - \exp(\sigma I_{\text{STED}})$. This dependence, shown by solid lines in Fig. 2(b), is seen to provide a reasonably accurate fit for the lock-in output measured as a function of the power of STED radiation for all the wavelengths of the STED field, indicating the predominance of one-photon transitions over multiphoton processes in the STED process in our experiments.

As the STED radiation wavelength is increased from 815 nm [filled circles in Fig. 2(b)] to 1210 nm [rectangles in Fig. 2(b)], the lock-in output monotonically decreases,
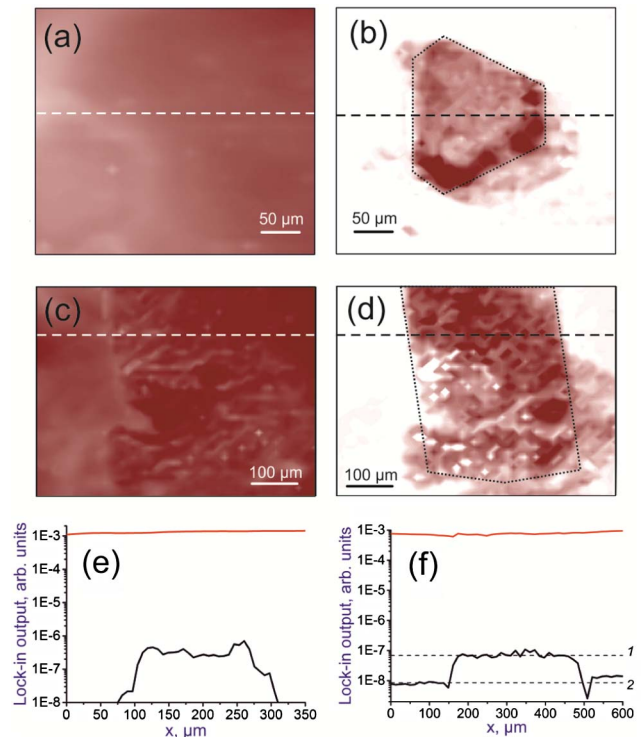
Fig. 3. Fluorescent images of an NV-diamond particle taken through (a),(b) a 1-mm-thick layer of rhodamine 6G solution and (c),(d) a 200 μm thick slice of mouse brain without (a), (c) and with (b),(d) TMSTED suppression of the fluorescence background. (e),(f) One dimensional cuts of these fluorescent images taken along the dashed lines shown in the panels with (black line) and without (red line) TMSTED suppression of the fluorescence background for an NV-diamond particle imaged through (e) rhodamine 6G solution and (f) a slice of mouse brain. The dashed lines show the median levels of (1) the TMSTED fluorescence intensity corresponding to NV diamond and (2) the TMSTED-suppressed background from the brain tissue. Contours of NV-diamond particles are shown with dotted lines.
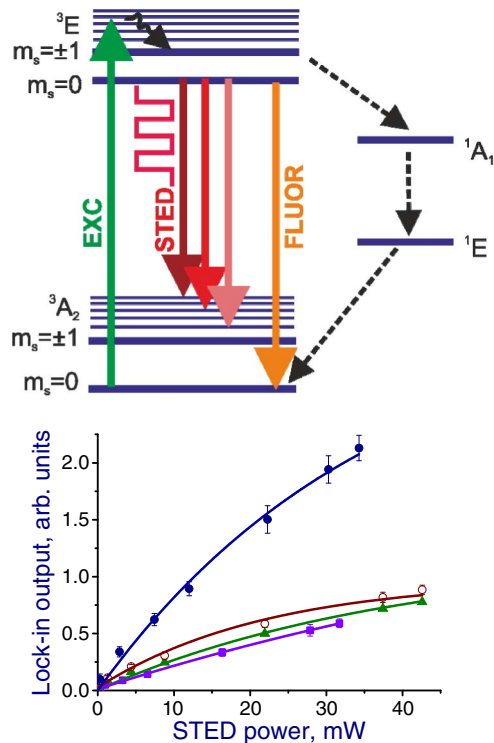

Fig. 2. (a) Diagram of the temporally modulated STED versus energy states of NV centers in diamond: Exc, excitation radiation; STED, frequency-tunable STED radiation; Fluor, fluorescence signal. (b) The lock-in output as a function of the STED radiation power for different STED radiation wavelengths: (filled circles) 815 nm, (open circles) 1064 nm, (triangles) 1110 nm, and (rectangles) 1210 nm. The best $S \propto 1 - \exp(\sigma I_{\text{STED}})$ fits are shown by solid lines.

indicating a monotonic drop in the efficiency of STED. This behavior is also fully consistent with the predominantly one-photon nature of STED transitions. Indeed, since the frequency of STED radiation ω remains lower than the frequency of a STED transition ω_{STED} within the entire STED-radiation tunability range [Fig. 2(a)], longer STED radiation wavelengths translate into larger frequency differences $\Delta\omega = \omega_{STED} - \omega$, lowering the efficiency of STED and decreasing the lock-in output in our experimental scheme. Based on these findings, the 815 nm output of a continuous-wave Ti: sapphire laser was used as a source of the STED radiation in all the experiments presented below in this Letter.

In the second set of experiments, NV diamond fluorescent markers were placed inside an aqueous solution of rhodamine 6G, which was used to mimic a strongly autofluorescent, albeit not strongly scattering medium. In a standard scheme of imaging, where the fluorescence signal is detected without any suppression of the fluorescent background, the fluorescence from a 1 mm thick layer of aqueous rhodamine 6G solution is three orders of magnitude more intense than the fluorescence of a single NV-diamond particle with a diameter of 250 μm used in this measurement. As a result, the NV-diamond particle is not visible in fluorescent images recorded without the STED beam [Fig. 3(a) and the red line in Fig. 3(e)]. When the temporally modulated STED field is on, on the other hand, the fluorescence background because of rhodamine 6G is suppressed by more than five orders of magnitude [see the red and black lines in Fig. 3(e)], through appropriate lock-in detection as described above, making the NV diamond particle clearly visible in the resulting fluorescent images [Fig. 3(b)]. Notably, no spectral filtering was applied in our experiments to separate the fluorescence resulting from NV diamond markers from the background luminescence, provided by dye molecules. The method of fluorescence contrast enhancement demonstrated in this experiment will thus work equally well for any spectrum of background fluorescence, including that of autofluorescence.

Finally, in the third series of experiments, the TMSTED technique was applied for brain imaging. In these experiments, a single NV-diamond particle with a diameter of 250 μm was placed beneath a 200 μm thick slice of a live brain sample extracted from a C57Bl-line mouse a few hours before an experiment. Brain slices were additionally colored with rhodamine to artificially increase the background in fluorescent images.

Fluorescent images recorded without a STED beam offer no clue with regard to the location of the NV-diamond particle [Fig. 3(c), red line in Fig. 3(f)]. With a temporally modulated STED field applied, the fluorescent background is reduced by five orders of magnitude, enabling the detection of the NV-diamond particle in fluorescent images [Fig. 3(d), black line in Fig. 3(f)]. An averaging time of 100 ms per pixel was found to be adequate for the conditions of our experiments. With such an averaging time and no *a priori* data on the location of NV diamond particles, images similar to the one shown in Fig. 3(d), synthesized of 50×50 pixels with a step of 7.4 μm, are fully recorded within about 20 minutes.

The contrast of these NV-diamond images can be quantified in terms of the ratio of the median levels of TMSTED fluorescence intensity corresponding to NV diamond [dashed line 1 in Fig. 3(f)] and TMSTED-suppressed background from the brain tissue [dashed line 2 in Fig. 3(f)]. For the image presented in Fig. 3(e), this contrast is estimated as $\eta \approx 120$. The lower efficiency of fluorescence background suppression provided by TMSTED and an excessive blurriness of NV-diamond images in experiments with brain slices compared to experiments with rhodamine solution are because of a strong scattering of brain tissues. The scattering length of brain slices used in our experiments, estimated as approximately 90 μm, was more than a factor of two shorter than the thickness of brain slices ($\approx$200 μm).

To summarize, we have demonstrated that modulation of STED in the time domain, combined with properly designed lock-in detection, can radically enhance the contrast of fluorescent images of strongly autofluorescent bio tissues. The temporally modulated STED technique, implemented with low-intensity continuous-wave laser sources, has been shown to provide an efficient all-optical suppression of a broadband fluorescent background, allowing the contrast of fluorescent images of mammal brain tissues tagged with nitrogen-vacancy diamond to be increased by five orders of magnitude.

References

1. T. Gaebel, M. Domhan, I. Popa, C. Wittmann, P. Neumann, F. Jelezko, J. R. Rabeau, N. Stavrias, A. D. Greentree, and S. Prawer, Nat. Phys. **2**, 408 (2006).
2. M. G. Dutt, L. Childress, L. Jiang, E. Togan, J. Maze, F. Jelezko, A. S. Zibrov, P. R. Hemmer, and M. D. Lukin, Science **316**, 1312 (2007).
3. T. M. Babinec, B. J. Hausmann, M. Khan, Y. Zhang, J. R. Maze, P. R. Hemmer, and M. Lončar, Nat. Nanotechnol. **5**, 195 (2010).
4. J. M. Taylor, P. Cappellaro, L. Childress, L. Jiang, D. Budker, P. R. Hemmer, A. Yacoby, R. Walsworth, and M. D. Lukin, Nat. Phys. **4**, 810 (2008).
5. J. R. Maze, P. L. Stanwix, J. S. Hodges, S. Hong, J. M. Taylor, P. Cappellaro, L. Jiang, M. G. Dutt, E. Togan, A. S. Zibrov, A. Yacoby, R. L. Walsworth, and M. D. Lukin, Nature **455**, 644 (2008).
6. G. Kucsko, P. C. Maurer, N. Y. Yao, M. Kubo, H. J. Noh, P. K. Lo, H. Park, and M. D. Lukin, Nature **500**, 54 (2013).
7. L. P. McGuinness, Y. Yan, A. Stacey, D. A. Simpson, L. T. Hall, D. Maclaurin, S. Prawer, P. Mulvaney, J. Wrachtrup, F. Caruso, R. E. Scholten, and L. C. Hollenberg, Nat. Nanotechnol. **6**, 358 (2011).
8. D. Le Sage, K. Arai, D. R. Glenn, S. J. DeVience, L. M. Pham, L. Rahn-Lee, M. D. Lukin, A. Yacoby, A. Komeili, and R. L. Walsworth, Nature **496**, 486 (2013).
9. I. V. Fedotov, L. V. Doronina-Amitonova, D. A. Sidorov-Biryukov, A. B. Fedotov, K. V. Anokhin, S. Y. Kilin, K. Sakoda, and A. M. Zheltikov, Appl. Phys. Lett. **104**, 083702 (2014).
10. T. Schröder, A. W. Schell, G. Kewes, T. Aichele, and O. Benson, Nano Lett. **11**, 198 (2011).

11. I. V. Fedotov, N. A. Safronov, Y. A. Shandarov, A. A. Lanin, A. B. Fedotov, S. Y. Kilin, K. Sakoda, M. O. Scully, and A. M. Zheltikov, Appl. Phys. Lett. **101**, 031106 (2012).
12. I. V. Fedotov, L. V. Doronina-Amitonova, A. A. Voronin, A. O. Levchenko, S. A. Zibrov, D. A. Sidorov-Biryukov, A. B. Fedotov, V. L. Velichansky, and A. M. Zheltikov, Sci. Rep. **4**, 5362 (2014).
13. X. Liu, J. Cui, F. Sun, X. Song, F. Feng, J. Wang, W. Zhu, L. Lou, and G. Wang, Appl. Phys. Lett. **103**, 143105 (2013).
14. I. V. Fedotov, L. V. Doronina-Amitonova, D. A. Sidorov-Biryukov, N. A. Safronov, S. Blakley, A. O. Levchenko, S. A. Zibrov, A. B. Fedotov, S. Y. Kilin, M. O. Scully, and A. M. Zheltikov, Opt. Lett. **39**, 6954 (2014).
15. I. V. Fedotov, S. Blakley, E. E. Serebryannikov, N. A. Safronov, V. L. Velichansky, M. O. Scully, and A. M. Zheltikov, Appl. Phys. Lett. **105**, 261109 (2014).
16. S. W. Hell, Nat. Biotechnol. **21**, 1347 (2008).
17. S. W. Hell, Nat. Methods **6**, 24 (2008).
18. C. Eggeling, C. Ringemann, R. Medda, G. Schwarzmann, K. Sandhoff, S. Polyakova, V. N. Belov, B. Hein, C. von Middendorff, A. Schönle, and S. W. Hell, Nature **457**, 1159 (2009).
19. E. Rittweger, K. Y. Han, S. E. Irvine, C. Eggeling, and S. W. Hell, Nat. Photonics **3**, 144 (2009).
20. K. Y. Han, K. I. Willig, E. Rittweger, F. Jelezko, C. Eggeling, and S. W. Hell, Nano Lett. **9**, 3323 (2009).
21. S. Arroyo-Camejo, M.-P. Adam, M. Besbes, J.-P. Hugonin, V. Jacques, J.-J. Greffet, J.-F. Roch, S. W. Hell, and F. Treussart, ACS Nano **7**, 10912 (2013).
22. E. C. Chen, O. Gaathon, M. E. Trusheim, and D. Englund, Nano Lett. **13**, 2073 (2013).
23. M. Dyba and S. Hell, Phys. Rev. Lett. **88**, 163901 (2002).
24. S. K. Sarkar, A. Bumb, X. Wu, K. A. Sochacki, P. Kellman, M. W. Brechbiel, and K. C. Neuman, Biomed. Opt. Express **5**, 1190 (2014).
25. R. Chapman and T. Plakhoitnik, Opt. Lett. **38**, 1847 (2013).